Engineering Structures 195 (2019) 568–578

Contents lists available at ScienceDirect

Engineering Structures

journal homepage: www.elsevier.com/locate/engstruct

Bond-slip modelling of reinforced concrete lap splices subjected to low and high strain rates

Eric Jacques[a,*], Murat Saatcioglu[b]

[a] Charles E. Via, Jr. Dept. of Civil and Environmental Engineering, Virginia Tech, Blacksburg, VA, United States
[b] Department of Civil Engineering, University of Ottawa, Ottawa, ON, Canada

A B S T R A C T

This paper presents an analytical model developed to predict the flexural load-deformation behavior of reinforced concrete members containing tension lap splices. The proposed model incorporates the effect of reinforcement slip of the lap splice and the effect of high strain rates on bond characteristics and material properties of concrete and steel. The main advantages of the proposed model are that bond-slip phenomena are captured through the use of pseudo-material stress-strain relationships, rather than giving consideration to the continuum of reinforcement and slippage over the entire structural element. Material properties and associated dynamic increase factors (DIF) are defined using accepted formulations. A suitable bond-slip law is presented and modified to account for the influence of strain rates on bond characteristics. Beam failure criteria are expressed in terms of a flexural failure of the member or a bond splitting failure of the splice. A comparison of the analytical predictions with experimental data demonstrated that the proposed analysis technique can reasonably predict the flexural response of beams with tension lap splices. The results also show that the model is equally applicable for use at low- and high- strain rate loading, such as those generated during blast and impact loading.

1. Introduction

The mechanism of force transfer between reinforcing steel and concrete, known as bond, is a fundamental characteristic of reinforced concrete behavior. This phenomenon is caused by the cumulative effect of surface friction, chemical adhesion and mechanical interlock of rebar lugs with concrete [1]. Considerable research over the past century has led to a thorough and exhaustive understanding of the factors affecting bond strength for the case of quasi-static loading [1]. However, little effort has been directed towards establishing the influence of high strain rates caused by short duration, dynamic loads on bond characteristics [2].

Strain rate ($\dot{\varepsilon}$), defined as the rate of change of strain with respect to time, typically varies from $10^{-5}\,s^{-1}$ for static loading and up to $10^{3}\,s^{-1}$ for hard impact and blast events [3]. Bond strength, like the constitutive material properties of steel and concrete, experiences an apparent enhancement due to high strain rate effects [4–6]. The degree of improvement is influenced by the quality of concrete [7,8], the size of reinforcement, and the presence of transverse reinforcement, in addition to being inversely proportional to an idealized crack splitting failure plane defined by the development length and the distance between the smallest concrete cover and the center of the developed bar [2]. In addition, confinement provided by transverse ties or increased cover depth, results in greater bond resistance but reduced strain rate sensitivity [8,9]. Concrete cover, in particular, has been shown experimentally and computationally to provide inertial confinement leading to increased bond force at high strain rates [10]. Recent research by Jacques [2] demonstrated that, on average, the total bond force developed in anchored/spliced reinforcement increased by a factor of 1.28 at strain rates on the order of $0.1–1.0\,s^{-1}$. However, Jacques also demonstrated that the assumption of perfect bond between steel and concrete at high strain rates is not entirely applicable since the flexural strength and stiffness of lap-spliced reinforced concrete beams was markedly less than that predicted using conventional flexural theory. This observation suggests that accounting for the bond-slip response of flexural reinforcement and the surrounding concrete can be critical when structures are subjected to extreme loads generated during blast and impact events.

The assumption of perfect bond, commonly used in design, is generally only valid for low load levels, prior to significant cracking of concrete [11]. This assumption becomes especially tenuous in regions of high stress transfer near cracks, where a difference in strain between steel and concrete occurs because of the relative displacement between the two materials. This relative displacement, known as bond-slip, can significantly alter the flexural response of reinforced concrete through several mechanisms, including: (i) tension stiffening [12]; (ii) anchorage slip [13]; and (iii) lap splice slippage/extension having the effect of softening the section and increasing the flexibility of the spliced

* Corresponding author.
E-mail addresses: ejacques@vt.edu (E. Jacques), murat.saatcioglu@uottawa.ca (M. Saatcioglu).

https://doi.org/10.1016/j.engstruct.2019.05.104
Received 9 December 2018; Received in revised form 12 April 2019; Accepted 31 May 2019

member [14].

Considerable effort has been directed towards developing analytical methods to describe the mechanics of bond-slip as it affects reinforced concrete flexural behavior. The most common approach reported in the literature for modelling partially-bonded reinforcement has been the use of flexibility-based fiber elements [15–18]. The flexibility-based method mathematically approximates a smooth steel stress distribution within anchored regions to simplify solution of the differential equations of equilibrium and compatibility of anchored/developed reinforcement. Other, simpler methods of approaching the bond-slip problem also exist, for example [19] incorporated bond-links into a moment-curvature analysis, while [13] computed rigid body end rotation of flexural members through integration of the strain distribution along anchored reinforcement. Although each of the studies selected an appropriate constitutive bond-slip relationship based on the type of reinforcement and expected failure mode, their scope was limited to static loading. To the best knowledge of the authors, no previous work has examined the effect of high strain rates on the flexural response of reinforced concrete experiencing reinforcement slippage and a partial loss of bond. Addressing this gap in the knowledge is especially important for advancing the state of the art of protective design to ensure the continued safety and resilience of concrete infrastructure.

This paper presents the development of an analytical model to predict the effect of reinforcement slippage of tension lap splices on the flexural behavior of reinforced concrete beams subjected to low and high strain rates. Details of the model are discussed, including an appropriate bond-slip law, material properties for steel and concrete, and dynamic increase factors (*DIF*) to account for rate effects. The effectiveness of the methodology was validated against comprehensive load-deformation data recorded during experimental testing of reinforced concrete beams subjected to four-point static tests and dynamic shock tube loading. The objective of the analytical study was to demonstrate that the response of tension lap splices subjected to dynamic loads can be predicted satisfactorily using the proposed analysis technique.

2. Methodology

This paper presents a procedure to consider the effect of slippage of spliced reinforcement using a pseudo stress-strain relationship for incorporating the bond-slip effect. The procedure is valid for low strain rate static loads, as well as high strain rate dynamic loading. The assumptions of plane strain and perfect bond form the basis of conventional reinforced concrete flexural analysis for which perfect bond necessitates compatibility between the strains in reinforcing steel (ε_s) and concrete (ε_c) such that $\varepsilon_c = \varepsilon_s$. Combined, the mathematical implication of the perfect bond assumption is that the strain at any location within a section (ε) is a function of the average strain (ε_{avg}), curvature (ϕ), and the distance from the neutral axis to the location under consideration (y) through the relation

$$\varepsilon_c = \varepsilon_s = \varepsilon = \varepsilon_{avg} - \phi y \tag{1}$$

In the proposed procedure, the assumption of perfect bond is relaxed, and steel is permitted to slip relative to the surrounding concrete. Therefore, strain compatibility requires that

$$\varepsilon_c = \varepsilon_s + \varepsilon_{slip} \tag{2}$$

where ε_{slip} is the slippage strain due to imperfect reinforced concrete bond.

Whereas values of ε_c and ε_s can be obtained directly from material stress-strain relationships, bond-slip expressions are required to obtain appropriate values for ε_{slip}. Consider the spliced region with length L_s subject to constant axial tension force $f_s A_b$ illustrated in Fig. 1. From the perspective of the observer, the starter bar and surrounding concrete are assumed fixed, while the spliced bar experiences a slip displacement (s) relative to the starter bar. Slippage of reinforcement leads to a reduction in the effective splice length available for bond transfer, expressed as $L_s' = L_s - s$. The slippage strain may now be defined as

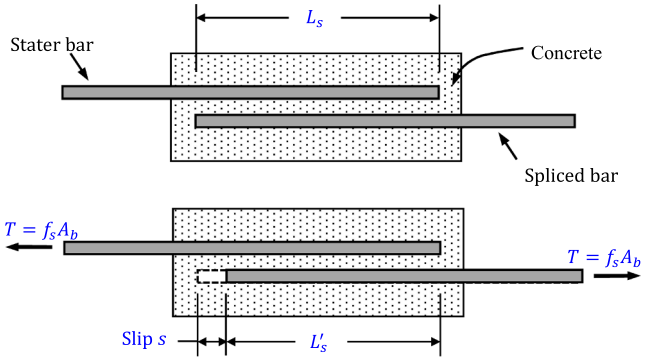

Fig. 1. Idealized reinforcement lap splice region.

$\varepsilon_{slip} = s/L_s$. The effective strain in reinforcement within the splice (ε_s'), incorporating the effects of bond-slip, can be conveniently written as

$$\varepsilon_s' = \varepsilon_s + \frac{s}{L_s} = \varepsilon_s + \varepsilon_{slip} \tag{3}$$

Assuming constant bond stress (u) in the splice, the steel stress developed over L_s' can be written as

$$f_s = \frac{u L_s' \pi d_b}{A_b} = \frac{4 u L_s'}{d_b} \tag{4}$$

provided that the values of ε_s and f_s satisfy compatibility with the stress-strain law for the bare reinforcing steel. It is evident from Eq. (4) that the effective steel stress developed within the splice is a function of the degree of reinforcement slippage and of the bond-slip characteristics of the steel-concrete interface. Therefore, a bond-slip law that accurately describes the transfer of interfacial stresses between the reinforcing bar and concrete is essential for tracing the evolution of steel stress within the splice as a function of rebar slippage.

The proposed model incorporates the segmental bond-slip law developed by Eligehausen et al. [20] modified using strain rate dependent parameters to describe the variation in bond strength and stiffness as a function of reinforcement slip expected to occur under dynamic conditions [21]. The envelope bond-slip curve, shown in Fig. 2, consists of four stages. The variation in bond stress during the ascending stage up to slip s_1 is:

$$u = u_m \left(\frac{s}{s_1}\right)^{\beta} \tag{5}$$

where u_m is the maximum bond stress corresponding to bond failure and the exponent β is used to calibrate the expression to experimental data. The second stage consists of a region of constant bond u_m until slip

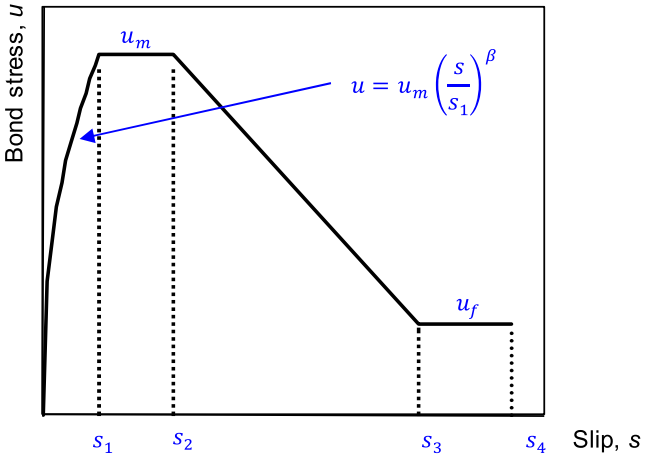

Fig. 2. Bond-slip relationship proposed by Eligehausen et al. [20].

s_2. The third stage, a descending branch of linearly decreasing bond up to slip s_3, is followed by a region of constant frictional bond u_f until incipient failure at s_4. The parameters used to define the segmental bond-slip law (*i.e.*, u_m, u_f, $s_{1\to4}$ and β), described in the following section, are typically selected to provide a suitable match with experimental bond-slip data [22].

The maximum bond stress corresponding to splice failure u_m was computed based on the ACI 408R [1] descriptive expression for the total bond force (T_b) generated in development and splice regions such that:

$$u_m = \frac{T_b}{\pi d_b L_s} \tag{6}$$

To account for dynamic strength increases on bond capacity, the expression for total bond force T_b (kN) in Eq. (5) was modified based on previous research which demonstrated that bond is sensitive to strength enhancement when subjected to blast and impact loading [5–9]. The strain rate sensitivity of bond strength is divided into three components, each affected by rapid loading [2], consisting of: the dynamic concrete strength in compression (f'_{dc}); the dynamic bond force developed without transverse reinforcement (T_{dc}); and the additional dynamic bond force developed when splices are confined by transverse reinforcement (T_{ds}). Using the ACI descriptive expression for static bond as a foundation [1], the dynamic total bond force (T_{db}) in developed or spliced reinforcement subjected to high strain rates can be expressed based on [2] as

$$T_{db} = T_{dc} + T_{ds} \tag{7}$$

where the concrete contribution to dynamic bond force is equal to the dynamic bond force that would be developed without transverse reinforcement is:

$$T_{dc} = DIF_{T_c} \times [1.43 L_s (c_{\min} + 0.5 d_b) + 57.4 A_b] \left(\frac{0.1 c_{max}}{c_{min}} + 0.9 \right) f'^{1/4}_{dc} \tag{8}$$

and the additional strength provided by the transverse reinforcement is:

$$T_{ds} = DIF_{T_s} \times \left(8.9 t_r t_d \frac{N A_{tr}}{n} + 558 \right) f'^{3/4}_{dc} \tag{9}$$

where:

- A_b is the bar area (mm^2);
- f_s is the steel stress at failure (MPa);
- f'_{dc} is the dynamic compressive strength of concrete (MPa);
- DIF_{T_c} is the dynamic increase factor which accounts for the apparent increase in bond force developed without transverse reinforcement;
- DIF_{T_s} is the dynamic increase factor which accounts for the apparent increase in the additional bond force provided by transverse reinforcement;
- L_s is the splice length (mm);
- c_b is the bottom cover to the bar being developed or spliced (mm);
- c_{so} is the side cover to the bar being developed or spliced (mm);
- c_{si} is ½ of the clear bar spacing (mm);
- c_s is the minimum of c_{so} and c_{si} + 6.35 (mm);
- c_{min} is the minimum of c_b or c_s (mm);
- c_{max} is the maximum of c_b and c_s (mm);
- d_b is the bar diameter (mm);
- h_r is the reinforcement rib height (mm);
- s_r is the reinforcement rib spacing (mm);
- R_r is the relative rib ratio, approximately equal to 0.8 to 0.9 h_r/s_r [1];
- t_r is the effect of relative rib area on T_s ($t_r = 9.6R_r + 0.28$);
- t_d is the effect of bar size on T_s ($t_d = 0.03 d_b + 0.22$);
- N is the number of transverse stirrups or ties within L_s;
- A_{tr} is the area of each stirrup or ties crossing a potential splitting plane adjacent to reinforcement being developed (mm^2), and;
- n is the number of bars being spliced.

An examination of the T_{db} given in Eqs. (7)–(9) indicates that the strain rate sensitivity of bond strength is a function of f'_{dc}, as well as the construction and geometric properties of the splice affecting DIF_{T_c} and DIF_{T_s}. For strain rates in the range of $0.1 \le \dot{\varepsilon} \le 1.2\ \mathrm{s}^{-1}$, the values of DIF_{T_c} and DIF_{T_s} can be computed using the relationships proposed by Jacques [2]:

$$DIF_{T_c} = -1.20 \times 10^{-5} L_s (c_{min} + 0.5 d_b) + 1.04 \times 10^{-3} A_b + 1.18 \ge 1.00 \tag{10}$$

$$DIF_{T_s} = 1.14 \tag{11}$$

which were developed from a database of 41 mostly unconfined splice tests conducted on reinforced concrete beams sampled at strain rates commonly associated with protective design. Eq. (10) indicates that the strain rate sensitivity of bond force for bars not confined by transverse reinforcement is proportional to bar area A_b and inversely proportional to an idealized failure plane defined by the development length and the distance between the smallest concrete cover and the center of the developed bar $L_s(c_{min} + 0.5 d_b)$. For splices with transverse reinforcement, a constant value of $DIF_{T_s} = 1.14$ was proposed based on a limited dataset for a narrow range of confinement ratios and relative rib geometries.

As has been discussed, the concrete stress-strain relation [Fig. 3(a)] exhibits an increase in strength and stiffness when subjected to high strain rate loading [23]. The dynamic compressive strength f'_{dc}, can be calculated following:

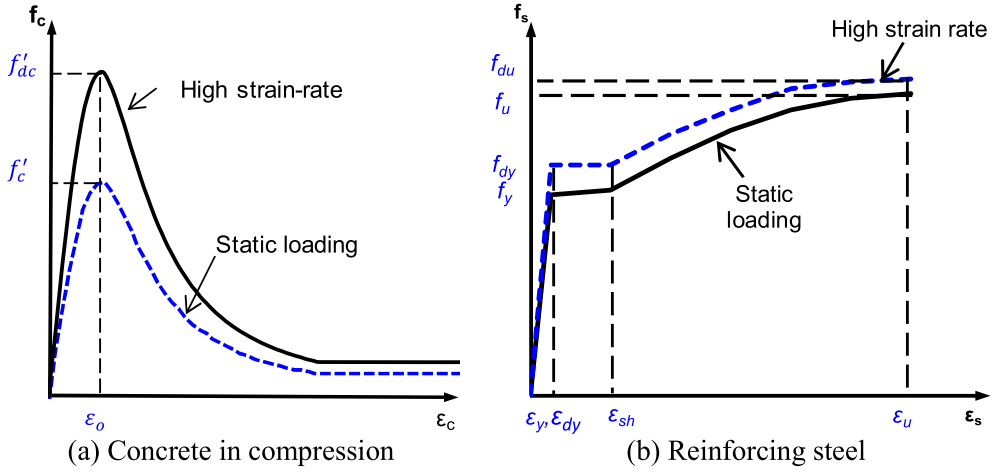

Fig. 3. Static and high strain rate stress-strain relationships used in the analytical model.

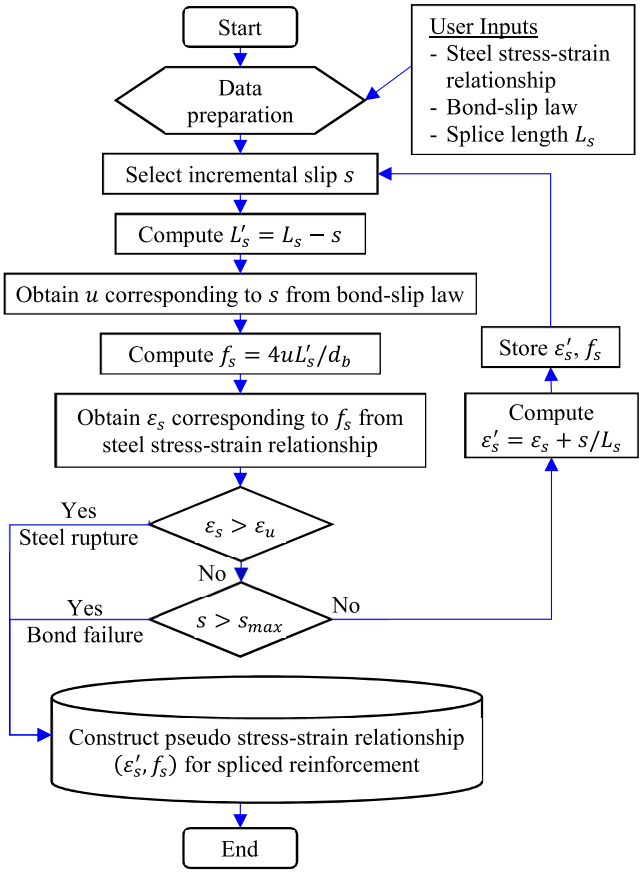

Fig. 4. Flowchart for the development of pseudo stress-strain relationships incorporating bond-slip response.

$$f_{dc}^{'} = DIF_{f_c} \times f_c^{'} \tag{12}$$

where DIF_{f_c} is the dynamic increase factor to account for high strain rate effects on concrete compressive strength, and $f_c^{'}$ is the static compressive strength. The 1990 CEB Model Code expression [24] is used to predict values of DIF_{f_c} for concrete in compression according to:

$$DIF_{f_c} = \left(\frac{\dot{\varepsilon}}{30 \times 10^{-6}}\right)^{1.026\alpha} \quad \text{for} \quad \dot{\varepsilon} \leq 30 \ \ \text{s}^{-1} \tag{13}$$

$$\alpha = \frac{1}{5 + \frac{9f_c^{'}}{10}} \tag{14}$$

Reinforcing steel, like concrete, experiences an increase in material properties due to dynamic loading. The strain rate sensitivity of reinforcing steel is inversely proportional to strength, with yield strength exhibiting greater sensitivity than ultimate strength [23]. The work of [25] can be used to obtain values of *DIF* for both f_y and f_u to construct dynamic stress-strain relationships from static data. As illustrated in Fig. 3(b), static stress-strain relationships for steel are modified by applying a linear variation in *DIF* to stress values between yield and ultimate. Strain rate and static yield strength were used as inputs to obtain values of *DIF* according to [25]:

$$DIF = \left(\frac{\dot{\varepsilon}_s}{10^{-4}}\right)^{\alpha} \tag{15}$$

valid for $10^{-4} \leq \dot{\varepsilon}_s \leq 225 \ \ \text{s}^{-1}$ and $290 \leq f_y \leq 710 \ \ \text{MPa}$.

The *DIF* applied to the static yield strength to obtain the dynamic yield strength

$f_{dy} = DIF_{f_y} \times f_y$ may be determined by substituing $\alpha = \alpha_{f_y}$ in Eq. (15) according to:

$$\alpha_{f_y} = 0.074 - \frac{0.040 f_y}{414} \tag{16}$$

A similar procedure was followed to obtain the dynamic ultimate strength $f_{du} = DIF_{f_u} \times f_u$ where $\alpha = \alpha_{f_u}$ is substituted in Eq. (15) as follows:

$$\alpha_{f_u} = 0.019 - \frac{0.009 f_y}{414} \tag{17}$$

Bond parameters governing the general shape of the segmental bond-slip law were likewise selected to represent bond behavior of reinforcing steel in concrete at high strain rates. The value of $\beta = 0.4$ reported by [20] and adopted in the Model Code [24] was used in this study as good correlation was reported between the shape of the initial ascending branch with experimental data for unconfined concrete under static loading. For elastic bond at high strain rates, Jacques and Saatcioglu [26] showed that the exponent β, used to calibrate the ascending branch of the bond-slip against experimental data, was insensitive to load rate for $\dot{\varepsilon} \approx 1 \ \text{s}^{-1}$ and that $\beta = 0.4$ reasonably captured the shape of the ascending branch for unconfined concrete. Bar slips $s_{1 \rightarrow 4}$, used to define transition points in the segmental bond curve, are commonly expressed in terms of the clear distance, s_L, between rebar lugs. The bar slips at the transition points were found to not be particularly sensitive to strain rate effects [26]. Values of slip proposed by [27] for unconfined reinforcement subjected to static loads, specifically $s_1 = 0.15 s_L$, $s_2 = 0.35 s_L$, $s_3 = s_L$, were adopted in this study and assumed valid for high strain rate loading case. Finally, the frictional bond stress u_f was assumed to be equal to $u_m/4$ [24].

Effective stress-strain relationships for spliced reinforcement, incorporating the effect of bond deterioration, can be obtained by solving Eqs. (3) and (4) for progressively increasing values of bar slip obtained from bond-slip expressions, whilst ensuring compatibility with the steel stress-strain relationship. The resulting pseudo-material property, whose characteristics are dependent on the size and grade of reinforcement, and of the construction of the splice itself, serve as a convenient mathematical representation of an otherwise complicated bond phenomenon. The advantage of this formulation is that the fundamental characteristics of bond-slip can be described using modified material properties in conventional sectional analysis. Note that while the procedure was developed for dynamic high strain rate loads, setting all values of $DIF = 1$ yields predictions for the static load case.

The analytical procedure to develop the stress-strain response of rebar including bond-slip effects subjected to high strain rates is described by the flowchart in Fig. 4. By assuming an incremental displacement field along the length of the spliced region, the effective load carrying capacity of the splice is computed by ensuring compatibility between the bond-slip and material stress-strain law, the latter derived from coupon test data or curve-fitting relationships. Information regarding the failure mechanism of the splice can also be obtained. A splice failure due to bond loss is likely to occur if rebar slip s exceeds the maximum bar slip s_{max} defined in the bond-slip law prior to steel stress ε_s exceeding the material rupture strain ε_u. Splice failure due to steel rupturing is predicted if $\varepsilon_s > \varepsilon_u$ is achieved prior to $s > s_{max}$.

Fig. 5 demonstrates the effect of bond-slip on spliced reinforcement for various levels of bond. For the case of superior bond conditions, the response of partially bonded reinforcement closely follows that of the bare rebar, with only a small decrease in initial stiffness due to low levels of slippage. As bond conditions deteriorate, the initially stiff bond-slip response follows the behavior of the perfectly bonded segment only for relatively low load levels. As stress in the splice is increased, slippage has the effect of reducing the effective strength and stiffness of reinforcement, while also limiting the maximum attainable strain. A splice failure, either by splitting or pull-out, is indicated when the ultimate strain defined in the effective stress-strain response is exceeded prior to achieving the ultimate rupture strain of the reinforcement. If the structural element provides a weak level of bond, (*e.g.*

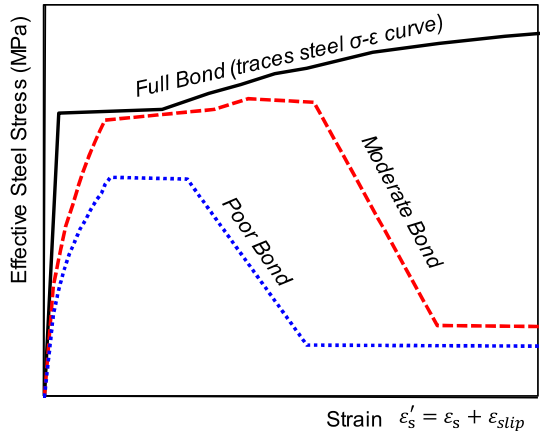

Fig. 5. Typical pseudo stress-strain relationship developed for different levels of bond.

insufficient cover depth or inadequate developed length) the stress-strain response of the spliced region is expected to closely follow the general shape of the bond-slip curve. In such cases, it is unlikely that the splice will develop the reinforcement yield strength and will exhibit considerably lower stiffness than what is expected for continuous reinforcement.

3. Brief description of experimental tests

The accuracy of the proposed model was evaluated by conducting an analytical study of the lap splice beams tested by [28]. The effectiveness of the pseudo stress-strain relationships at predicting the global strength and stiffness of lap spliced beams was compared against static and dynamic tests.

A total of 22 large-scale reinforced concrete beams, divided into 11 companion pairs of nominally identical specimens, were tested. One beam from each pair was tested statically, while the other was subjected to dynamic loading were generated using the University of Ottawa Shock Tube and load application device [2], illustrated in Fig. 6(a). Simply supported four-point bending tests was used, with a clear span of 2232 mm and two symmetrical load points generating a 744 mm long constant moment region. Strain rates on the order of $\dot{\varepsilon} \approx 1$ s^{-1} were achieved during dynamic tests, while $\dot{\varepsilon} \approx 10^{-5}$ s^{-1} were obtained statically.

The cross-section and geometry of the tests is illustrated in Fig. 6(b and c). Construction details and material properties are summarized in Table 1. The test variables consisted of the size of longitudinal reinforcement, cover depth, concrete strength, and the presence of transverse reinforcement (confined or unconfined splices). The splices were proportioned to fail once the reinforcement achieved a stress of 400 MPa. Displacement transducers recorded the mid-span deflection, while load cells placed in the supports were used to obtain reaction forces. Dynamic analysis was performed to compute the internal member resistance based on equilibrium of reaction load cell readings, applied pressure distribution and inertia of the beam system. In addition, strain gauges (SG) were installed on the spliced reinforcement to obtain the distribution of stress within each spliced bar at the locations indicated in Fig. 6(d). Each bar was instrumented with a strain gauge placed at mid-splice and another placed outside of the spliced length, but within the constant moment region. This configuration allowed the development of strains within the spliced and non-spliced regions of reinforcement to be monitored. The gauges were oriented along the neutral axis of the reinforcement and care was taken to ensure the installation of the strain gauges and placement of lead wires did not significantly disturb the integrity of the splices. The reader is directed to other studies [2,28] for further information about the tests.

4. Analytical study

An analysis of the behavior of lap splice beams subjected to static and dynamic loading was generated using sectional analysis to obtain the moment–curvature ($M{\cdot}\phi$) relations, followed by member analysis to obtain the load-deflection response. The first step in the analytical procedure was to establish the static material properties for steel and concrete at the appropriate loading rate.

A series of linear and parabolic segments fit to coupon test data was used to represent the stress-strain relationship for the reinforcement [30]. The stress-strain curves used reinforcement at high strain rates was constructed by applying appropriate values of *DIF* steel [Eqs. (15)–(17)] established using the $\dot{\varepsilon}$ observed during the tests.

The Thorenfeldt et al. [29] uniaxial stress-strain model was used for unconfined concrete in compression using cylinder data for $f_c^{'}$ (Table 1). The model was modified to account for high strain rate loading by applying appropriate values of *DIF* to $f_c^{'}$ [Eqs. (13) and (14)] established using the $\dot{\varepsilon}$ observed during the tests. The expression for the ascending and descending branches is given as follows:

$$f_c = \frac{f_c^{'} \cdot n \cdot \left(\frac{\varepsilon_c}{\varepsilon_o}\right)}{n - 1 + \left(\frac{\varepsilon_c}{\varepsilon_o}\right)^{nk}} \tag{18}$$

in which calibration constants n, ε_o, k were computed as follows:

$$n = 0.8 + \frac{f_c^{'}}{17} \tag{19}$$

$$\varepsilon_o = \frac{f_c^{'}}{E_c} \times \frac{n}{n - 1} \tag{20}$$

$$E_c = 3320\sqrt{f_c^{'}} + 6900 \tag{21}$$

$$k = \begin{cases} 1 & \text{for} \frac{\varepsilon_c}{\varepsilon_o} \le 1.0 \\ 0.67 + \frac{f_c^{'}}{62} & \text{for} \frac{\varepsilon_c}{\varepsilon_o} > 1.0 \end{cases} \tag{22}$$

The stress-strain curves used for high strain rate response of concrete in compression were constructed by applying appropriate values of *DIF* for concrete [Eqs. (13) and (14)] and steel [Eqs. (15)–(17)], established using the $\dot{\varepsilon}$ observed during the tests.

The tensile stress-strain curve for concrete was modelled following the work of Bentz [12]. The initial ascending portion up to first cracking was represented by a linear curve with slope given by the initial tangent stiffness of concrete given in Eq. (21). The peak tensile cracking strength of concrete (f_{cr}) was taken as

$$f_{cr} = 0.45(f_c^{'})^{0.4} \tag{23}$$

The second portion of the tensile curve, accounting for tension stiffening of concrete which can occur after first cracking, was expressed following:

$$f_t = \frac{f_{cr}}{1 + \sqrt{3.6m{\cdot}\varepsilon_t}} \tag{24}$$

where the parameter $m = A_c / \sum d_b \pi$ accounts for the influence of bond characteristics on the area of concrete in tension (A_c) by the perimeter of all the reinforcing bars in the area ($\sum d_b \pi$).

The dynamic tensile strength of concrete (f_{dcr}) was computed by applying a dynamic increase factor, $DIF_{f_{cr}}$ to account for the effect of high strain rates on the tensile properties of concrete as follows:

$$f_{dcr} = DIF_{f_{cr}} \times f_{cr} \tag{25}$$

where $DIF_{f_{cr}}$ was defined according to the formulation proposed by Malvar and Crawford (1998b). They defined the dynamic increase factor for concrete strength in tension as:

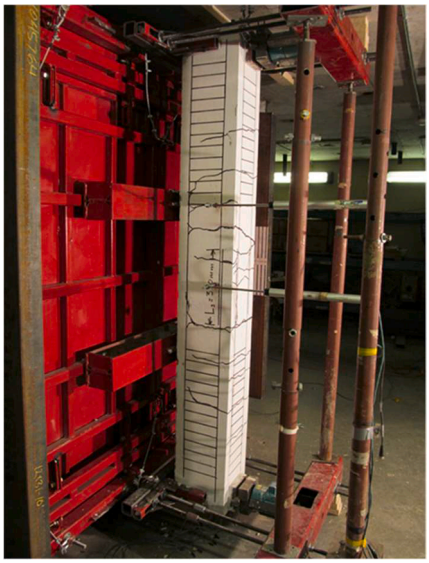

(a) Shock tube test fixture

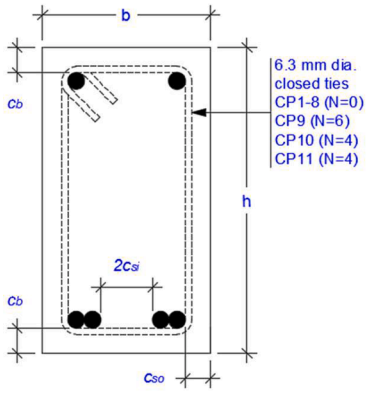

(b) Cross-section through spliced region

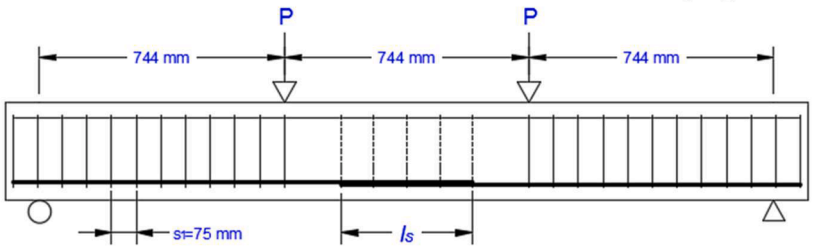

(c) Elevation view of lap splice beam specimens

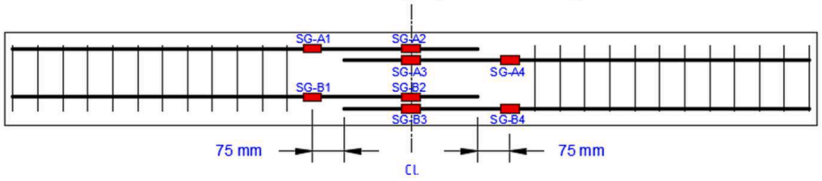

(d) Strain gauage positioning on splice reinforcement

Fig. 6. Specimen details of the lap splice beams tested by [2].

$$DIF_{f_{cr}} = \begin{cases} \left(\frac{\dot{\varepsilon}}{10^{-6}}\right)^{\delta} & \text{for } \dot{\varepsilon} \le 1s^{-1} \\ \beta\left(\frac{\dot{\varepsilon}}{10^{-6}}\right)^{\frac{1}{3}} & \text{for } \dot{\varepsilon} > 1s^{-1} \end{cases} \tag{26}$$

$$\delta = \frac{1}{1 + \frac{8f_c^{'}}{10}} \tag{27}$$

$$\log\beta = 6\delta - 2 \tag{28}$$

Having established the constitutive stress-strain relations of the base materials, the effective stress-strain relationship for spliced reinforcement incorporating bond-slip effects was constructed following the procedure outlined in Fig. 4 and described in Section 2.

Next, two $M{\cdot}\phi$ relationships were established for each beam: one for regions of fully-bonded reinforcement and the other for regions of partially-bonded spliced reinforcement. Both $M{\cdot}\phi$ relationships were constructed with the same geometric configuration and concrete constitutive material properties. However, the $M{\cdot}\phi$ relationship for fully-bonded reinforcement was developed with the bare steel stress-strain curve, while the $M{\cdot}\phi$ for spliced reinforcement was developed using the effective stress-strain bond-slip element. The $M{\cdot}\phi$ analysis was performed by imposing an incremental curvature on the cross-section and iterating on the neutral axis depth. Equilibrium of forces was achieved considering the sum of internal stresses computed at 150 integration points. The $M{\cdot}\phi$ analysis was terminated when reinforcing steel strain exceeded the material rupture strain or the effective bond splitting failure strain of reinforcement as defined by either the bare bar or effective bond-slip stress-strain curves.

Bending moment was assumed to be the dominant action in the member analysis performed to construct the load-deflection curve incorporating reinforcement slippage, while the effect of shear and axial forces were neglected. Each beam was discretized into 160 segments along its length, resulting in a spacing of approximately 14 mm between segments. This equates to the lap splices being discretized between roughly 11 and 30 segments for the range of L_s values considered in this study. This was found to provide satisfactory results since the bending moment, and hence curvature, in the spliced region was constant for the four-point bending test arrangement. Note that the analyst is cautioned to perform a mesh sensitivity study to confirm convergence of their member discretization for combinations of boundary conditions, load arrangement, and cross-sectional configuration other than those considered in this research.

Once the member was discretized, a small, incremental load was applied to compute the bending moment at the midpoint of each segment. The curvature for segments having fully bonded reinforcement was mapped onto the beam from the $M{\cdot}\phi$ relationship developed for fully-bonded reinforcement, while the curvature for segments located in

Table 1
Construction and reinforcing details of lap splice beams.

Specimen Designation	$f_c'^*$ MPa	f_y^* MPa	b mm	h mm	d_b mm	A_b mm^2	c_b mm	c_{so} mm	c_{si} mm	L_s mm	n	N	A_{tr} mm^2
CP1-LSR	32.5	431.2	150	200	11.3	100	26	27	37	275	2	–	–
CP1-HSR	42.9	559.2					27	25	39	276			
CP2-LSR	32.5	431.2	240	200	11.3	100	51	49	60	168	2	–	–
CP2-HSR	42.7	557.4					52	49	60	160			
CP3-LSR	32.5	448.4	165	300	16.0	200	26	24	43	493	2	–	–
CP3-HSR	43.8	587.0					26	26	41	494			
CP4-LSR	32.5	448.4	265	300	16.0	200	52	52	65	272	2	–	–
CP4-HSR	44.6	597.0					51	50	67	282			
CP5-LSR	48.7	448.4	165	300	16.0	200	28	27	40	409	2	–	–
CP5-HSR	60.0	585.6					27	25	42	395			
CP6-LSR	48.7	448.4	265	300	16.0	200	53	52	65	235	2	–	–
CP6-HSR	60.3	590.3					51	47	70	230			
CP7-LSR	32.5	491.0	280	300	19.5	300	53	54	67	415	2	–	–
CP7-HSR	44.1	623.4					52	55	66	397			
CP8-LSR	48.7	491.0	280	300	19.5	300	53	54	67	360	2	–	–
CP8-HSR	60.2	622.3					51	53	68	361			
CP9-LSR	36.9	448.4	165	300	16.0	200	25	28	39	325	2	6	62.4
CP9-HSR	48.3	588.3					24	27	40	327			
CP10-LSR	36.9	448.4	265	300	16.0	200	48	52	65	187	2	4	62.4
CP10-HSR	47.3	574.1					49	50	67	185			
CP11-LSR	45.2	448.4	265	300	16.0	200	49	48	69	164	2	4	62.4
CP11-HSR	55.7	574.9					53	48	69	175			

* Material properties for high strain rate tests multiplied by appropriate *DIF*.

the spliced region was established from the partially-bonded $M{\cdot}\phi$ diagram. Mid-span deflection was then computed by numerical integration of the curvature distribution $\phi(x)$ along the length of the beam such that $\Delta = \int_0^{L/2} \phi(x){\cdot}x{\cdot}dx$. The total load, mid-span deflection and steel stress in the lap splice were stored for later use. A new incremental applied load was then selected, and the procedure was repeated. The stopping criterion defined in the analysis was when the beam mid-span moment exceeded the moment capacity of the lap splice, which meant that post-peak behavior was not considered in the present analysis. Piecewise linear functions were then constructed describing the load-deflection response and the variation in stress in the lap splice as a function of applied load. The predicted behavior of the beams was then compared against experimentally obtained data.

5. Results and discussion

A comparison of experimental and predicted beam resistance curves for companion pairs CP4, CP6, CP8, and CP10 at low and high strain rates is shown in Fig. 7, while plots comparing all 22 beams can be found in [2,28]. To assess the significance of bond-slip on flexural response, the analysis was also performed considering the case of perfect bond between reinforcing steel and concrete, which have been presented for comparison in Fig. 7. Results of the analysis for the case of partial-bond are reported in Table 2. The experimental and predicted quantities compared include: the peak resistance (R_{exp} and R_{pred}, respectively) and peak resistance ratios (R_{pred}/R_{exp}); the displacement at peak resistance (δ_{exp} and δ_{pred}) and displacement ratios ($\delta_{pred}/\delta_{exp}$), and; the splice stress at peak resistance ($f_{s,exp}$ and $f_{s,pred}$) and splice stress ratios ($f_{s,pred}/f_{s,exp}$).

With regard to the experimental resistance curves shown, the peak strength of beams tested at high strain rates was in all cases significantly greater than the strength of beams subjected to slowly applied static loading. This characteristic, common for structures subjected to short duration, dynamic loads [23,28,31], can be attributed to an apparent increase in material strength due to rate effects. Fig. 7 show that the fully- and partially-bonded flexural analyses yield reasonably good predictions of the peak strength of the lap splice beams for the cases of low and high strain rates. Furthermore, partial-bond flexural predictions, incorporating appropriate material *DIF*s, were able to capture the initially very rigid behavior of the high strain rate beams. The results suggest that the expressions for *DIF* applied to concrete properties and steel reinforcement, in addition to the Jacques expression [2] for dynamic bond strength [*i.e.* Eqs. (7)–(11)], can be relied upon to provide reasonable predictions of the ultimate strength of flexural members subjected to high strain rate loading.

A focused comparison of experimental stress developed in the splice against splice stress predicted using fully- and partially-bonded analysis techniques is shown in Fig. 8(a) and (b) for the low and high strain rate specimen from companion pair CP4, respectively. Experimental splice stress was obtained by converting strain readings taken in the constant moment region – but outside the spliced zone – into stress using appropriate steel stress-strain relations. In general, the comparisons indicate that the fully-bonded flexural analysis does not adequately capture the evolution of stress in splices which undergo reinforcement slip as a function of member resistance. Reinforcement slip deformations in the spliced region increase the net tensile strain at the level of the reinforcement This decreases the depth of the neutral axis and increases the cross-sectional curvature required to maintain equilibrium of internal forces. This increase in curvature has a detrimental effect on the distribution of internal stresses along the height of the section, which results in a decrease in moment capacity for the same effective reinforcement stress. As a result, spliced reinforcement experiencing slippage must develop a greater level of stress to achieve the same internal restoring moment than fully-bonded continuous reinforcement. The partially-bonded analysis method proposed herein can reasonably capture the effect of varying degrees of splice slippage on the flexural behavior of the test samples and appears to be equally applicable for low and high strain rates.

Good agreement between predicted and experimental data was obtained when the phenomenology of bond-slip in lap-spliced reinforcement was expressed through the use of an effective reinforcement stress-strain relationship. A comparison between the experimental and predicted peak resistances is plotted in Fig. 9 (a), with comparisons grouped according to strain rate. A mean peak resistance ratio (R_{pred}/R_{exp}) of 0.97 (coefficient of variation, COV = 10%) was obtained for the partial-bond analysis of all 22 tests. No significant statistical difference was observed in the accuracy of the predictions of peak resistance conducted at low or high strain rates. Similarly, the stress in the splices at failure was predicted with a reasonably good level of accuracy as illustrated in Fig. 9(b): the mean splice stress at peak resistance ratio $f_{s,pred}/f_{s,exp}$ for all twenty-two tests was 0.93 with a COV of

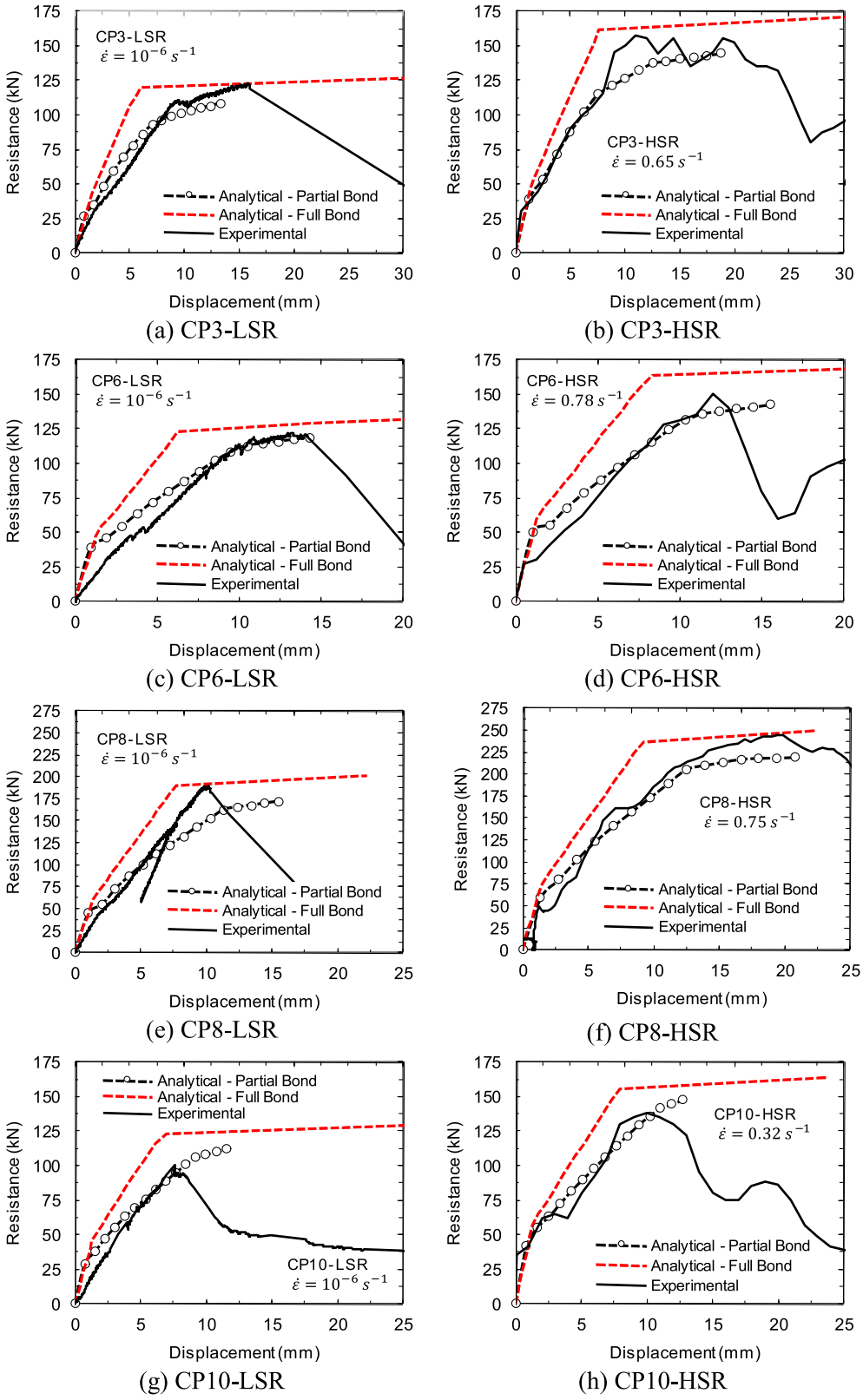

Fig. 7. Comparison of low and high strain rate experimental resistance curves against those predicted considering full- and partial-bond conditions for splices not confined.

6%.

Unlike predictions of peak resistance and splice stress, the predictions of the displacement corresponding to splice failure were predicted with a lower level of accuracy. The mean ratio of $\delta_{pred}/\delta_{exp}$ for all tests was 1.14 (COV = 32%). However, the peak displacement for low strain rate tests were consistently overestimated (Average $\{\delta_{pred}/\delta_{exp}\}_{LSR} = 1.29$), which could be attributed to the choice of bond-slip model used in the analysis, while the same quantities for high strain

Table 2
Comparison of experimental and predicted low and high strain rate results for the case of partial bond.

Beam	Strain rate $\dot{\varepsilon}$	Peak Resistance			Displacement at peak resistance			Splice stress at peak resistance		
		R_{exp} (kN)	R_{pred} (kN)	$\frac{R_{pred}}{R_{exp}}$	δ_{exp} (mm)	δ_{pred} (mm)	$\frac{\delta_{pred}}{\delta_{exp}}$	$f_{s,exp}$ (MPa)	$f_{s,pred}$ (MPa)	$\frac{f_{s,pred}}{f_{s,exp}}$
CP1-LSR	1.5×10^{-5}	38.4	37.0	0.96	14.8	17.9	1.21	457	430	0.94
CP1-HSR	0.31	47.7	46.9	0.98	50.7	19.5	0.38	575	534	0.93
CP2-LSR	1.8×10^{-5}	45.6	41.4	0.91	25.8	23	0.89	468	446	0.95
CP2-HSR	0.28	52.0	50.7	0.98	66.8	20.5	0.31	602	544	0.90
CP3-LSR	7.0×10^{-6}	122.9	108.4	0.88	16.0	13.3	0.83	462	404	0.87
CP3-HSR	0.65	155.0	144.5	0.93	19.0	18.8	0.99	585	539	0.92
CP4-LSR	5.5×10^{-6}	114.6	109.4	0.95	9.6	13.4	1.40	458	409	0.89
CP4-HSR	1.13	164.0	141.4	0.86	15.6	15.4	0.99	570	531	0.93
CP5-LSR	4.1×10^{-6}	130.6	122.5	0.94	10.0	13.4	1.34	485	417	0.86
CP5-HSR	0.60	153.2	138.5	0.90	14.1	14.8	1.05	584	511	0.88
CP6-LSR	6.3×10^{-6}	121.6	118.4	0.97	14.1	14.3	1.01	467	410	0.88
CP6-HSR	0.78	149.8	142.4	0.95	12.2	15.5	1.27	588	512	0.87
CP7-LSR	7.6×10^{-6}	182.4	159.9	0.88	8.7	14.6	1.68	491	433	0.88
CP7-HSR	0.80	245.0	202.8	0.83	20.3	15.7	0.78	623	548	0.88
CP8-LSR	4.3×10^{-6}	185.5	171.8	0.93	10.1	15.5	1.53	491	434	0.88
CP8-HSR	0.75	244.0	218.8	0.90	20.0	20.8	1.04	604	561	0.93
CP9-LSR	1.3×10^{-5}	109.2	117.9	1.08	9.5	12.7	1.34	426	441	1.04
CP9-HSR	0.70	154.4	156.7	1.01	11.1	17.6	1.59	585	584	1.00
CP10-LSR	7.4×10^{-6}	100.1	112.0	1.12	7.6	11.5	1.51	423	411	0.97
CP10-HSR	0.32	135.5	147.4	1.09	10.1	12.8	1.27	571	553	0.97
CP11-LSR	6.0×10^{-6}	99.4	117.1	1.18	7.4	11.3	1.53	417	416	1.00
CP11-HSR	0.33	134.5	153.1	1.14	11.0	13.9	1.26	561	561	1.00

rate tests were predicted with markedly improved accuracy (Average $\{\delta_{pred}/\delta_{expd}\}_{HSR} = 0.99$). Despite some inaccuracy in predicting the displacement at splice failure, the selected comparisons presented in Fig. 7 show that the partial-bond resistance curves can accurately trace the evolution of flexural strength and stiffness over the entire displacement range up to failure. This justifies the analysis procedure for prediction of member response for lap spliced beams subjected to static and dynamic loading with $\dot{\varepsilon}$ in the range of $10^{-5}\,s^{-1}$ and $1\,s^{-1}$.

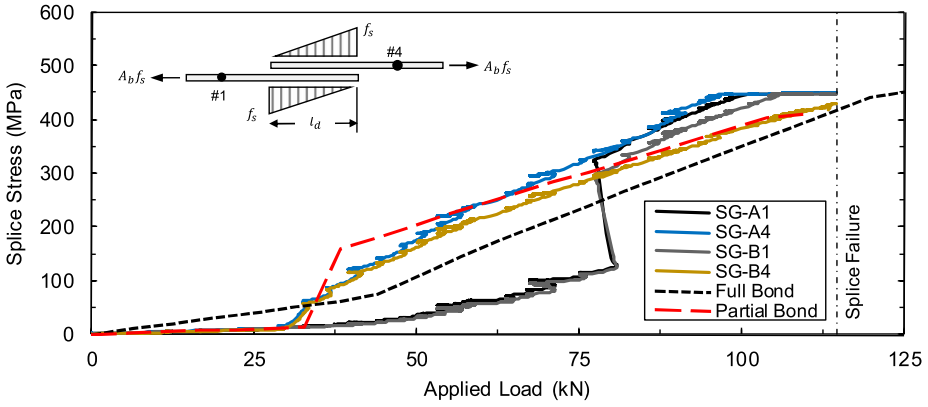

(a) CP4-LSR

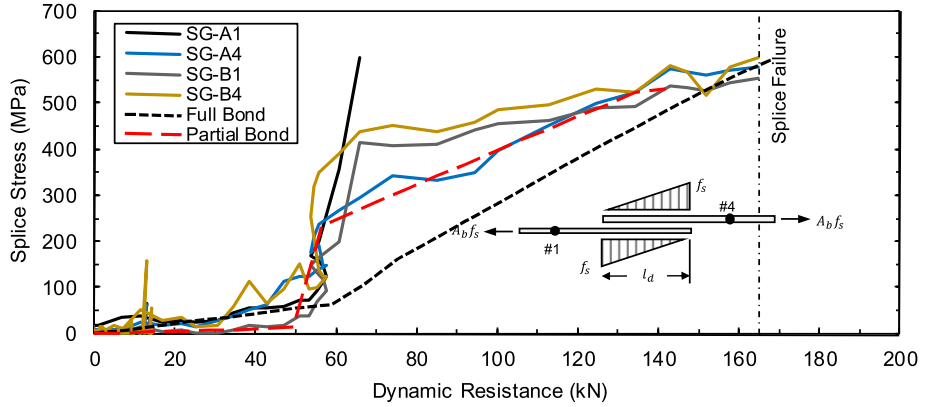

(b) CP4-HSR

Fig. 8. Comparison of experimental and predicted splice stress for companion pair CP4.

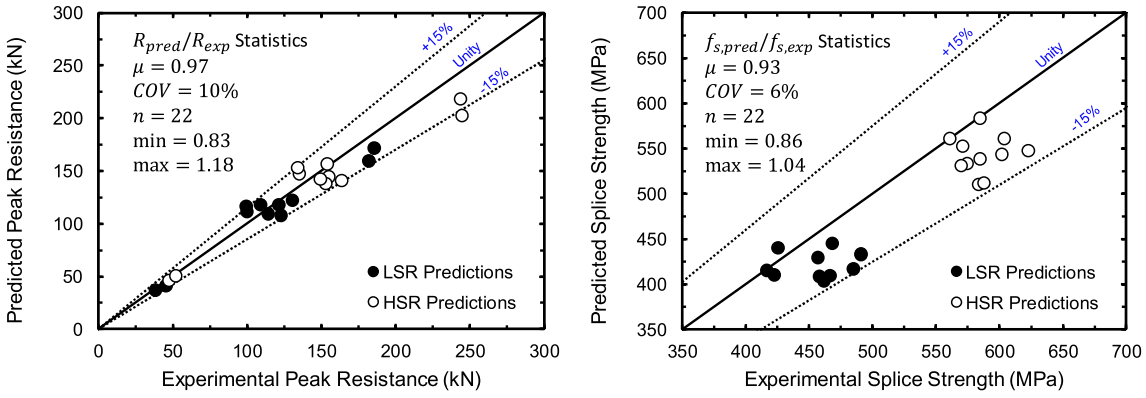

(a) Peak resistance (b) Splice stress at peak resistance

Fig. 9. Summary statistics for the proposed for the partially-bonded analysis methodology.

Another important observation was the influence of transverse reinforcement on flexural response. A comparison of the fully bonded flexural predictions against experimental data demonstrated that the effect of bond-slip was more pronounced for splices not confined by transverse reinforcement, as was the case for results illustrated in Fig. 7(a–f). However, the effect of reinforcement slip was reduced for the case of splices with transverse reinforcement (*i.e.* Fig. 7g and h). The improvement in member stiffness observed for beams having splices confined by transverse reinforcement was due to a passive clamping pressure provided by the transverse reinforcement which resists splitting of the cover concrete [1].

The results presented in this paper demonstrate that effective steel stress-strain relationships, incorporating partially-bonded reinforcement response, provide an acceptable means of capturing the fundamental characteristics of bond-slip along the splice length. By tailoring the selection of bond-slip law and key parameters (*i.e.*, peak bond strength and key slip points), the analyst can generate pseudo stress-strain relations for reinforcement in spliced regions having a range of superior or inferior bond conditions. The major advantages of the methodology are that it can provide reasonably accurate predictions and can be conveniently incorporated into existing moment-curvature or finite element software.

In some cases, however, the analytical model did underestimate flexural stiffness, for example, CP7-LSR and CP8-LSR. This could be attributed to the use of an empirical formulation for slip parameters [27], which are based on reinforcement lug spacing, which provide unrealistically large slips for the case of larger bars. In this regard, the slip parameters and overall shape of the bond-slip relation could be tuned to enhance the predictions generated by the proposed methodology. In addition, the methodology also had difficulty predicting the significant splice ductility exhibited by CP1-HSR and CP2-HSR. Despite these minor variances, the shape of the partially-bonded predictions showed much better correlation with experimental data that did the fully-bond predictions in all cases. Furthermore, the analysis does provide the opportunity for some future refinements. For example, the use of a local bond-slip model developed specifically to trace evolution of bond stress for developed/spliced bars susceptible to splitting failures, such as the one described by [27] could be investigated. In addition, post-peak load-deflection curves could also be generated provided a suitable solution scheme is implemented thus providing additional information on the splice behavior after peak bond stress has been attained. Finally, further validation is required to assess the suitability and limitations of the methodology when applied to a broader range of reinforced concrete flexure members containing tension lap splices than those considered in this study.

6. Summary and conclusions

An analytical model was presented which could predict the flexural behavior of reinforced concrete members constructed with tension lap splices. The model incorporated the effect of slippage of the lap-spliced reinforcement, in addition to accounting for the effect of high strain rates on material and bond properties. The effectiveness of the methodology was validated against comprehensive resistance curve data recorded during experimental testing of reinforced concrete beams subjected to four-point static and dynamic shock tube loading. Good agreement between experimental and predicted displacement responses was obtained when considering a condition of partial-bond within the spliced region. Additional analyses were also conducted to demonstrate that conventional, fully-bonded reinforced concrete flexural analysis over-predicted the strength and stiffness characteristics of the lap-spliced beams at both low and high strain rates. The results clearly demonstrated that the response of reinforced concrete beams with tension lap splices subjected to static and dynamic loads can be predicted satisfactorily using the proposed partial-bond analysis technique. However, further study is required to assess the suitability and limitations of the methodology when applied to a broader range of reinforced concrete members containing lap splices.

Acknowledgements

This research was funded by the Chemical, Biological, Radiological or Nuclear Research and Technology Initiative (CRTI) of Canada Projects CRTI-06-0150TD and CRTI-07-0176TD.

References

[1] ACI. ACI Committee 408: bond and development of straight reinforcing bars in tension. Farmington Hills, Michigan: American Concrete Institute; 2003.
[2] Jacques E. Characteristics of reinforced concrete bond at high strain rates PhD. Thesis Ottawa, Ontario: Department of Civil Engineering, University of Ottawa; 2016. p. 344.
[3] Bischoff PH, Perry SH. Compressive behaviour of concrete at high strain rates. Mater Res Soc Symp Proc 1991;64:151–65.
[4] Rezansoff T, Bufkin MP, Jirsa JO, Breen JE. The performance of lapped splices under rapid loading Research Report 154-2 Austin Texas: Center for Highway Research, The University of Texas at Austin; 1975 p. 104.
[5] Vos E, Reinhardt HW. Influence of loading rate on bond behaviour of reinforcing steel and prestressing strands. Mater Struct 1982;15(85):3–10.
[6] Yan C. Bond between reinforcing bars and concrete under impact loading PhD. Thesis Vancouver, B.C.: Department of Civil Engineering, University of British Colombia; 1992. p. 412.
[7] Shah IK, Hansen RJ. Behavior of bond under dynamic loading. Cambridge Massachusetts: Department of Civil Engineering, Massachusetts Institute of Technology; 1963.
[8] Solomos G, Berra M. Rebar pullout testing under dynamic Hopkinson bar induced impulsive loading. Mater Struct 2010;43(1–2):247–60.
[9] Weathersby JH. Investigation of bond slip between concrete and steel reinforcement

under dynamic loading conditions PhD. Thesis Baton Rouge, Louisiana: Department of Civil and Environmental Engineering, Louisiana State University and Agricultural and Mechanical College; 2003. p. 280.
[10] Panteki E, Máca P, Häussler-Comb U. Finite element analysis of dynamic concrete-to-rebar bond experiments in the push-in configuration. Int J Impact Eng 2017;106:155–70.
[11] Gan Y. Bond stress and slip modeling in nonlinear finite element analysis of reinforced concrete structures MA.Sc. Thesis Toronto, Ontario: Graduate Department of Civil Engineering, University of Toronto; 2000. p. 269.
[12] Bentz EC. Sectional analysis of reinforced concrete members PhD. Thesis Toronto, Ontario: Department of Civil Engineering, University of Toronto; 2000. p. 310.
[13] Alsiwat JM, Saatcioglu M. Reinforcement anchorage slip under monotonic loading. J Struct Eng Am Soc Civil Eng, ASCE 1992;118(9):2421–38.
[14] Pimanmas A, Thai DX. Response of lap splice of reinforcing bars confined by FRP wrapping: application to nonlinear analysis of RC column. Struct Eng Mech 2011;37(1):111–29.
[15] Monti G, Filippou FC, Spacone E. Finite element for anchored bars under cyclic load reversals. J Struct Eng 1997;123(5):614–23.
[16] Ayoub A, Filippou FC. Mixed formulation of bond-slip problems under cyclic loads. ASCE J Struct Eng 1999;125(6):661–71.
[17] Monti G, Spacone E. Reinforced concrete fiber beam element with bond-slip. J Struct Eng 2000;126(6):654–61.
[18] Orakcal K, Chowdhury SR. Bond slip modeling of reinforced concrete columns with deficient lap splices. Proceedings of the 15th world conference on earthquake engineering 2012 (15WCEE), Lisbon, Portugal, September 24–28. 2012.
[19] Xiao Y, Ma R. Seismic retrofit of RC circular columns using prefabricated composite jacketing. ASCE J Struct Eng 1997;123(10):1357–64.
[20] Eligehausen R, Popov EP, Bertero V. Local bond stress-slip relationships of deformed bars under generalized excitations Rep. No. UCB/EERC 83/23 Berkeley: Earthquake Engineering Research Center, University of California; 1983.
[21] Vos E. Influence of loading rate and radial pressure on bond in reinforced concrete: a numerical and experimental approach PhD. Thesis The Netherlands: Delft University of Technology; 1983. p. 250.
[22] Ciampi V, Eligehausen R, Bertero VV, Popov EP. Analytical model for deformed bar bond under generalized excitations. Delft, The Netherlands: IABSE Colloquium on Advanced Mechanics in Reinforced Concrete; 1981.
[23] Department of Defense. Structures to Resist the Effects of Accidental Explosions. United Facilities Code (UFC) 03-340-02. Washington, D.C.: United States of America Department of Defense; 2008.
[24] CEB-FIP. Model Code 90 for Concrete Structures, Federation International de la preconstraint, CEB Bulletin No. 213/214, Paris; 1993.
[25] Malvar LJ, Crawford JE. Dynamic increase factors for steel reinforcing bars. In: Proceedings of the Twenty-Eighth DDESB Seminar, DoD Explosives Safety Board, Orlando, Florida; 1998a.
[26] Jacques E, Saatcioglu M. High strain rate response of reinforced concrete beam-ends. Int J Prot Struct 2018.
[27] Harajli MH, Hamad B, Karam K. Bond-slip response of reinforcing bars embedded in plain and fiber concrete. ASCE J Mater Civil Eng 2002;14(6):503–11.
[28] Jacques E, Saatcioglu M. High strain rate response of reinforced concrete lap splice beams. ASCE J Struct Eng 2018.
[29] Thorenfeldt E, Tomaszewicz A, Jensen JJ. Mechanical properties of high strength concrete and application in design. In: Proceedings of the Symposium Utilization of High Strength Concrete, Tapir, Trondheim; 1987, p. 149–59.
[30] Jacques E, Lloyd A, Saatcioglu M. Predicting reinforced concrete response to blast loads. Can J Civ Eng 2012;40(5):427–44.
[31] Lloyd AEW. Blast retrofit of reinforced concrete columns PhD. Thesis Ottawa, Ontario: Department of Civil Engineering, University of Ottawa; 2015. p. 466.